Energy Engineering

Tech Science Press

https://doi.org/10.32604/ee.2026.087353

ARTICLE

One-Step Electrodeposited Binder-Free MnO_2-NiO–rGO Composite for High-Performance Supercapacitor Electrodes

Masoumeh Ghalkhani[1,*], Hamidreza Mohammad Hoseini[1,2], Javad Beheshtian[2,*] and Rüstem Keçili[3]

[1]Electrochemical Sensors Research Laboratory, Department of Chemistry, Faculty of Science, Shahid Rajaee Teacher Training University, Lavizan, Tehran, Iran

[2]Department of Chemistry, Faculty of Science, Shahid Rajaee Teacher Training University, Lavizan, Tehran, Iran

[3]Department of Medical Services and Techniques, Yunus Emre Vocational School of Health Services, Anadolu University, Eskişehir, Türkiye

*Corresponding Authors: Masoumeh Ghalkhani. Email: ghalkhani@sru.ac.ir; Javad Beheshtian. Email: j.beheshtian@sru.ac.ir

Received: 15 June 2026; Accepted: 20 July 2026; Published: 12 November 2026

ABSTRACT: The development of efficient, low-cost, and scalable electrode materials is vital for advancing high-performance supercapacitors. Despite recent progress, many fabrication routes remain complex, expensive, or dependent on polymer binders that reduce conductivity and long-term stability. Therefore, the objective of this study was to develop a simple, binder-free electrode with enhanced electrochemical performance. In this work, we report a one-step electrodeposition method for fabricating a manganese nickel oxide–reduced graphene oxide (MnO_2-NiO–rGO) composite electrode directly on nickel foam. This facile technique employs an aqueous suspension of graphene oxide (GO) enriched with nickel and manganese salts, enabling the simultaneous formation of a three-dimensional porous network without any binder or additional reducing agent. Structural and morphological analyses conducted via X-ray diffraction (XRD), scanning electron microscopy (SEM), energy-dispersive X-ray spectroscopy (EDX), and elemental mapping confirmed the successful formation of a well-integrated nanocomposite. Electrochemical evaluations using cyclic voltammetry, galvanostatic charge–discharge, impedance spectroscopy, and cycling tests revealed that the optimized MnO_2-NiO–rGO composite exhibits a specific capacitance of 462.5 F/g at a current density of 5 A/g. The porous architecture enhances ion accessibility and promotes efficient charge storage and rapid transport. Notably, the electrode demonstrated excellent long-term stability, retaining 94% of its initial capacitance after 1000 cycles in alkaline electrolyte. These results highlight the potential of the MnO_2-NiO–rGO composite as a promising candidate for next-generation energy storage applications.

KEYWORDS: Carbon nanostructure; manganese oxide; supercapacitor; reduced graphene oxide; electrodeposition

1 Introduction

Environmental concerns, and accordingly the rising need for green and sustainable energy, have seriously focused researchers' attention on the development of cheaper energy production, conversion, and storage systems based on environmentally friendly strategies [1–3]. Energy storage systems used as storage or distributors of energy play an important role in industrial applications [4,5]. High energy and power density, long life span, good reversibility, and safety are the main criteria for making an energy storage instrument [6]. The electrochemical storage and energy conversion systems include batteries, supercapacitors, and fuel cells [7]. In batteries and fuel cells, the incumbent energy is generated by means of redox processes that transform chemical energy into electrical output [8]. In the closed system of batteries, the cathode and anode

Copyright © 2027 The Authors. Published by Tech Science Press. This work is licensed under a Creative Commons Attribution 4.0 International License, which permits unrestricted use, distribution, and reproduction in any medium, provided the original work is properly cited.

play the critical role that contributes to the redox reaction along with the energy conversion process [9]. Nevertheless, in fuel cells, the cathode and anode act as a substrate for the charge transfer process, for which the required active ingredients are continuously supplied from the outside of the cell [10,11]. In other words, they include an open system [12]. Rechargeable batteries, especially lithium batteries, are prevalent and usable because of their high energy density and good longevity [13]. However, they have limitations such as low power density, relatively high internal resistance, and low transmission power at high currents [14–16]. Supercapacitors are being developed by the majority of researchers as an efficient energy storage system [17,18]. Supercapacitors or electrochemical capacitors have received much attention due to their high cyclic life, low charging time and low internal resistance, high safety, and power density. On average, energy density in supercapacitors is enhanced by a factor ranging from 10 to 100 compared to that of electrolytic capacitors and can charge much faster than batteries [19]. In supercapacitors, energy is stored through the orientation of the ions in the electrochemical double layer at the electrode/electrolyte boundary, which is accompanied by the parallel configuration of electrons in the electrode substrate [20–22]. At the discharge time, the presence of charges at the electrode–electrolyte boundary induce the potential difference between the cathode and the anode [23]. Therefore, it transfers the stored charge to the external circuit. The high capacity of the supercapacitors stems from the high effective surface area of the electrode constituents and energy storage mechanism [24,25].

Wang et al. worked on the structure of nickel hydroxide and it synthesis on graphene oxide sheets and employed it for the construction of supercapacitors [26]. They achieved a specific capacitance of 1335 F/g. The results showed a massive mutation in the capacitance value of the graphene nanocomposites with metal oxides. Xiang et al. reported 472 F/g capacity for the supercapacitor prepared by coating Co_3O_4 on the rGO sheets. It showed 90% of its initial stability after 1000 cycles, revealing its significant cyclicity compared to similar works [27]. Liao et al. developed a flexible electrode by growing Co_3O_4 nanoparticles on vertically aligned graphene nanosheets deposited onto carbon fabric. The capacity of 580 F/g and 86% stability were reported after 20,000 charge/discharge cycles [28].

One-step electrochemical precipitation of the composite of graphene and metal oxides or metal hydroxides has great importance because of its simplicity and time-saving process. Zhao et al. settled the carbon sheets using electrochemical precipitation of manganese-GO composite [29]. The electrochemical storage capacity of the supercapacitor was greatly increased after the usage of the prepared composite. This process achieved a specific capacity of 829 F/g and a current density of 1.0 A/g. García-Gómez et al. recently co-deposited cobalt oxides and r-GO on a stainless steel bed using a one-step electrochemical technique. The optimized procedure led to the achievement of the specific capacity of 608 F/g at a current density of 0.1 A/g and increased reversibility that was much better than the electrode constructed solely by cobalt oxide [30]. Li et al. fabricated an electrode based on graphene nanosheets/nickel sulfide nanoparticles (GNs/Ni_3S_2) at high temperatures. The synthesized composite provided a specific capacitance of 652.5 F at 1.0 A/g with charge-discharge stability of 93% after 2000 cycles [31]. A nanostructure of NiO nanowires grown on NiO nanosheets was prepared by An et al. using Ni foam and a hydrothermal process [32]. They achieved a specific capacitance of 1349 F/g, with good stability. Xiao et al. grew NiO nanoflakes on Ni foam through hydrothermal reaction and achieved a specific capacitance of 870 mF/cm^2 [33]. Inamdar et al. fabricated a porous NiO film based on the chemical bath deposition reaction and obtained a specific capacitance of 69.8 F/g [34]. Chiku et al. applied a galvanostatic oxidation process to form NiO layers on the nickel sheets. The prepared electrode had a specific capacitance of 88 F/g [35].

2 Materials and Methods

2.1 Chemicals Materials

Manganese chloride hexahydrate, nickel chloride hexahydrate, sodium hydroxide, sodium nitrate, and graphite were supplied by Merck Company (Germany). The nickel foam (99% pure) was purchased from Nano Bazar Company in Iran.

2.2 Instruments

Electrochemical measurements were conducted using a Potentiostat/Galvanostat (SAMA 500, electro-analyzer system, I. R. Iran). To clean the electrode surface and prepare modifier suspensions, an ultrasonic bath (Pars Nahand Engineering Co., model PARASONIC 2600s) was employed. The morphology of the products was analyzed via scanning electron microscopy (SEM) with both a Philips El30 and a Tescan FE-SEM electron microscope. Electrochemical impedance spectroscopy (EIS) and charge-discharge testing were carried out with a VersaSTAT 4 Potentiostat/Galvanostat. The electrochemical setup consisted of a three-electrode system, with platinum wire, Ag/AgCl (saturated KCl), and nickel foam electrodes functioning as the auxiliary, reference, and working electrodes, respectively.

2.3 Synthesis of GO

The modified Hummer method was used to synthesize GO, in which graphite was used as the primary material. At first, 2.0 g of graphite was measured and transferred into a beaker, followed by the gradual addition of 50 mL of concentrated sulfuric acid to the beaker. Then, 2.0 g of sodium nitrate was added and the solution was stirred for an hour in the ice bath while its temperature was kept between 0°C to 5°C. After that, 5.0 g of potassium permanganate was incrementally introduced to the stirred solution over two hours. Subsequently, the temperature was increased to 35°C, and the mixture was stirred for an additional two hours at this temperature. At this stage, 46.0 mL of D.I. water was introduced to the reaction container, the temperature was raised to 90°C, and the mixture was stirred for 30 min. Next, 140 mL of double-distilled water was again added, and finally, 16 mL of 30% hydrogen peroxide was added. Subsequently, the reaction content was sonicated in the ultrasonic bath for one hour. The derived suspension was washed 3–4 times with D.I. water and then filtered using a Buchner funnel. Afterwards, the final sediment was rinsed several times with double-distilled water, and finally, the obtained brown solid material was dried overnight under vacuum conditions at 70°C.

2.4 Preparation of the Nickel Foam

The nickel foam was cut into 1 cm × 2 cm pieces. To remove the surface contamination from the nickel foam, it was subsequently sonicated in acetone, ethanol, and water for 15 min and was dried in the oven at 70°C.

2.5 Preparation of the GO Suspension

To prepare GO suspension (one mg/mL), 50 mg of synthesized GO was dispersed in 50 mL of D.I. water with the aid of two hours of magnetic stirring, followed by four times sonication in an ultrasonic bath, each one for 10 min.

2.6 Electrochemical Synthesis on the Nickel Foam

The electro-deposition solution was prepared by dissolving 0.1454 g of manganese chloride, 0.07 g of nickel chloride, and 0.424 g of sodium nitrate in 50 mL of D.I. water that was sufficiently stirred to obtain

a homogenous solution. The addition of $NaNO_3$ as a supporting electrolyte improves the ionic conductivity of the deposition bath and helps regulate the electrochemical deposition process by minimizing undesirable effects associated with excessive hydrogen evolution under negative potentials.

The cleaned nickel foams were immersed in a suspension of GO and purged with nitrogen gas for 10 min to remove the oxygen from the reaction solution. Then, four different modified Ni foam electrodes were fabricated by applying twenty cyclic voltammetry (CV) cycles in the potential range of −0.5 to −1.5 V, at different sweep rates (50, 100, 150, 200 mV/s). Here, the GO was converted to rGO under negative potential, and at the same time, it was precipitated on the surface of the nickel foam. The prepared electrode by this method was named rGO/NiFE. Then, rGO/NiFEs were washed with deionized water and inserted in the salt solution prepared from manganese chloride, nickel chloride, and sodium nitrate and the above steps were repeated. At last, the electrodes were placed in the oven overnight at 70°C, and then the electrodes were put in the furnace at 300°C for 2 h. The Ni foams modified with nano-composites of MnO_2, NiO, and rGO under CV scan rates of 50, 100, 150, and 200 mV/s were named as MnO_2-NiO–rGO50/NiFE, MnO_2-NiO–rGO100/NiFE, MnO_2-NiO–rGO150/NiFE, and MnO_2-NiO–rGO200/NiFE, respectively.

3 Discussion and Results

3.1 Characterization of the Prepared Samples

The crystal structure of the prepared MnO_2-NiO–rGO/NiFE was investigated by X-ray diffraction (XRD). The diffraction pattern was recorded over the 2θ range of 10°–80°, as shown in Fig. 1. The major diffraction peaks were observed at 2θ values of 36.94°, 42.77°, 44.21°, 51.56°, 62.72°, and 76.10°. According to the search–match analysis, the diffraction peaks at 36.94°, 42.77°, and 62.72° are consistent with cubic NiO (ICDD PDF No. **00-004-0835**), while the intense peaks at 44.21°, 51.56°, and 76.10° correspond to the (111), (200), and (220) planes of face-centered cubic nickel (ICDD PDF No. **98-004-8754**), originating from the nickel foam substrate. In addition, weak matches with carbon (ICDD PDF No. **01-079-1473**) and manganese (ICDD PDF No. **98-008-9933**) were obtained from the search–match analysis. However, no distinct diffraction peaks corresponding exclusively to crystalline MnO_2 or rGO were observed, which may be attributed to their low crystallinity and overlap with the strong diffraction peaks of the nickel substrate.

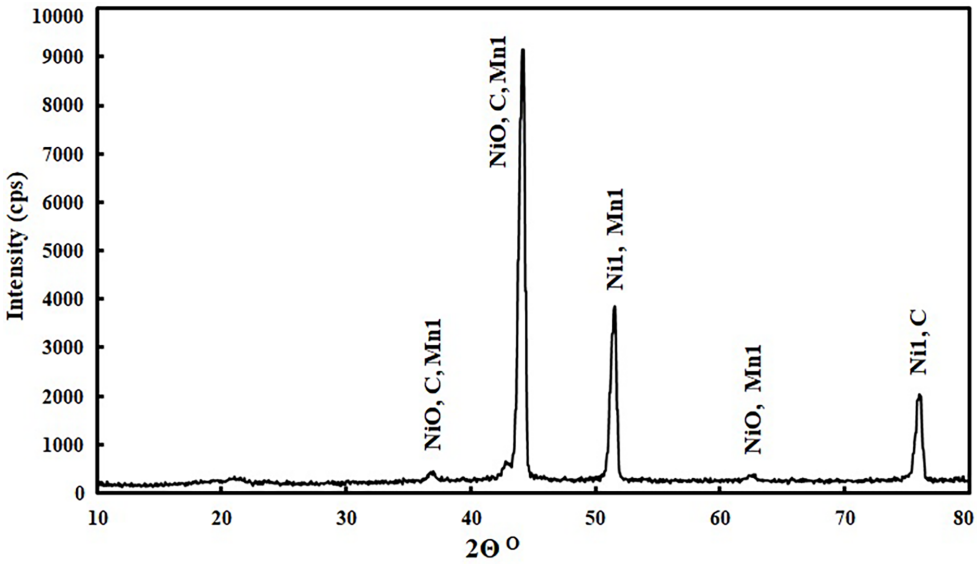


Figure 1: X-ray pattern of the prepared MnO_2-NiO–rGO/NiFE.

The surface morphology of the MnO_2-NiO–RGO/NiFE was examined by scanning electron microscopy (SEM). As shown in Fig. 2, the SEM image indicates that the MnO_2–NiO–rGO nanocomposite was successfully electrodeposited on the surface of the nickel foam. The deposited layer exhibits a rough and porous morphology, which is favorable for providing a large electroactive surface area for electrochemical reaction.

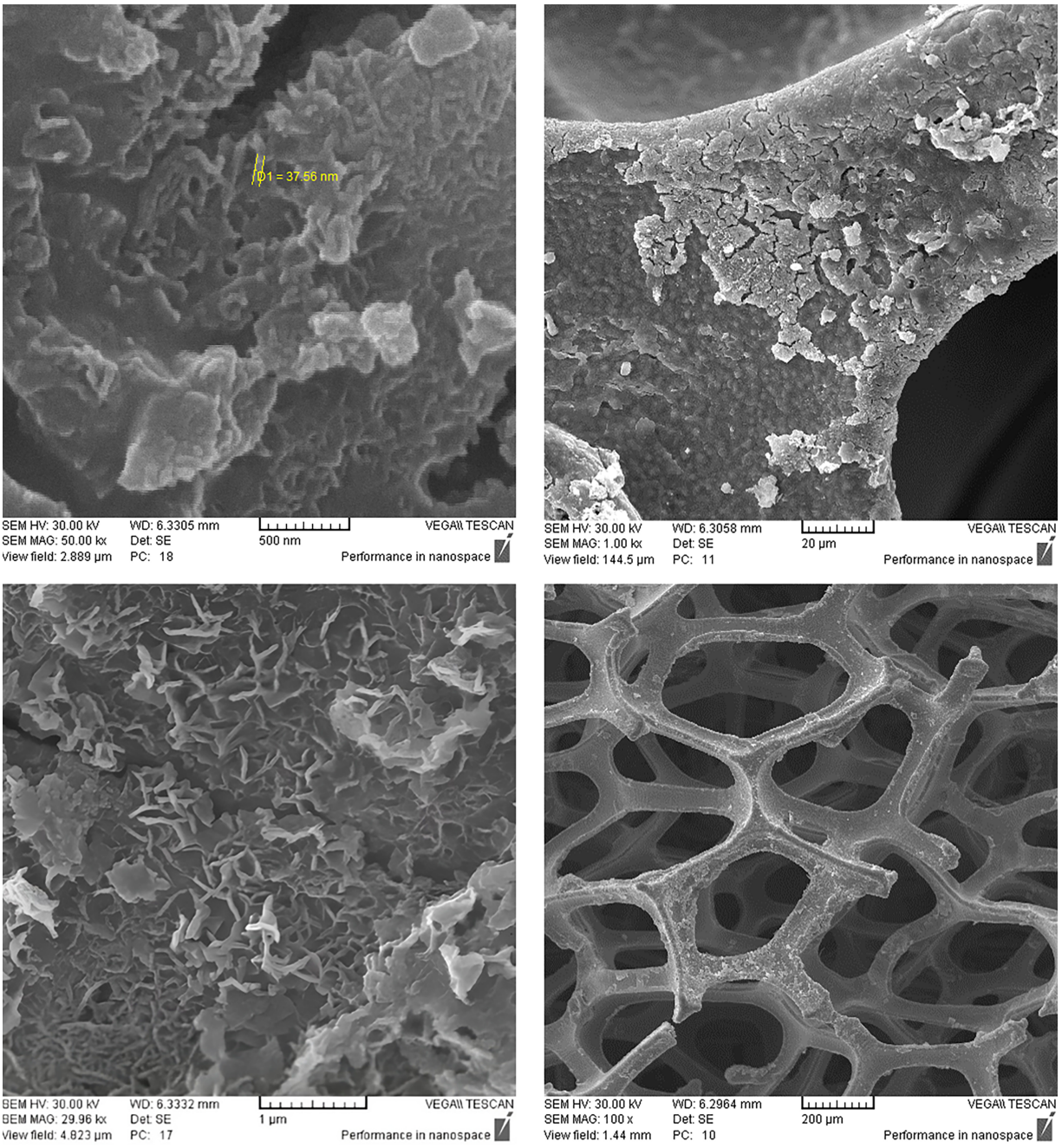


Figure 2: SEM images of the Ni foam electrochemically modified with a nanocomposite of MnO_2-NiO–rGO.

The elemental composition of the deposited MnO_2-NiO–rGO nanocomposite was analyzed by energy-dispersive X-ray spectroscopy (EDX). As shown in Fig. 3, the EDX spectrum confirms the presence of Ni, Mn, O, and C elements in the modified electrode. The Ni signal originates from both the nickel foam substrate

and the deposited NiO layer, while the Mn, O, and C signals verify the presence of manganese-containing species and reduced graphene oxide in the deposited nanocomposite. These results support the successful deposition of the MnO_2–NiO–rGO nanocomposite on the nickel foam.

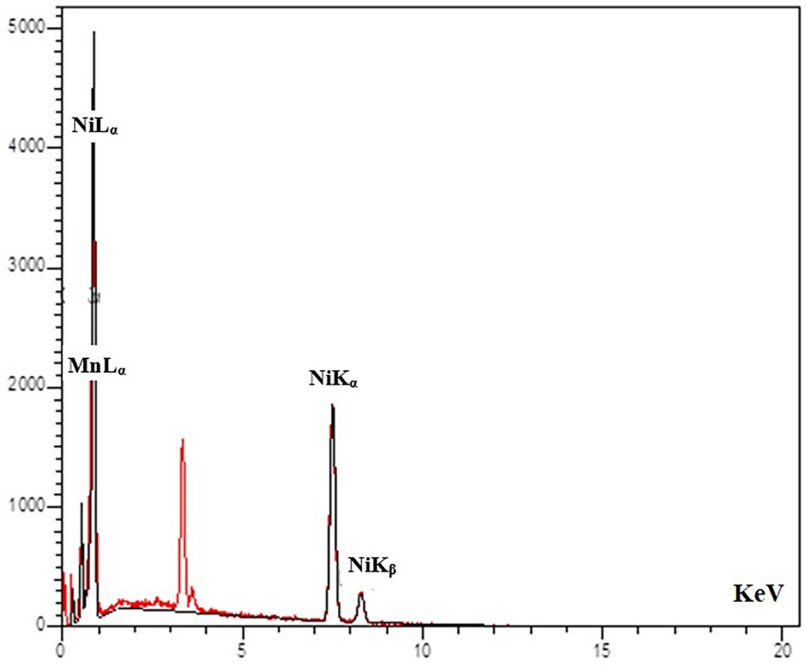


Figure 3: The EDX pattern obtained from the surface of the Ni foam electrochemically modified with a nanocomposite of MnO_2-NiO–rGO.

3.2 Electrochemical Studies

3.2.1 Cyclic Voltammetry Evaluations

To determine Faradic and non-Faradic behavior and to determine the amount of capacitance property of the fabricated electrode, the cyclic voltammetry (CV) method was applied. The most ideal electrode modified with a nanocomposite film as a supercapacitor electrode is the one that benefits from both the high stability and extended specific capacitance. The impact of the potential sweep rate of the CV method during the electro-modification of the NFEs was assessed by preparing MnO_2-NiO–rGO/NiFE under scan rates of 50, 100, 150, and 200 mV/s. Then, prepared electrodes were immersed in KOH solution and CVs recorded under wide range of sweep rates in the potential window of 0.0–0.5 V. During the the electrochemical measurements in alkaline KOH electrolyte, the charge storage mechanism of the NiO-containing electrode is associated with reversible surface redox transformations. Although NiO is identified as the crystalline phase after calcination, it can interact with the alkaline electrolyte and form electrochemically active hydroxide/oxyhydroxide species. The corresponding Faradaic process can be expressed as Eq. (1):

$$Ni(OH)_2 + OH^- \rightleftharpoons NiOOH + H_2O + e^- \quad (1)$$

Similarly, the MnO_2 component contributes to the pseudocapacitive behavior through a reversible proton-coupled electron transfer process (Eq. (2)):

$$MnO_2 + H_2O + e^- \rightleftharpoons MnOOH + OH^- \quad (2)$$

The obtained data represent that the electrode modified with a sweep rate of high potential at the stage of composite deposition on the nickel foam had the highest capacitance (Fig. 4). This behavior can be attributed to the formation of a more favorable surface morphology with accessible active sites and improved electrolyte penetration within the deposited composite layer. The electro-deposition of the composite on nickel foam by CV at a high velocity of potential sweep decreases the total duration of each cycle. As a result, the amount of total deposited material in each cycle decreases. According to the results, the fabricated electrode by nanocomposite deposition under a scan rate of 200 mV showed the highest specific capacitance (Table 1).

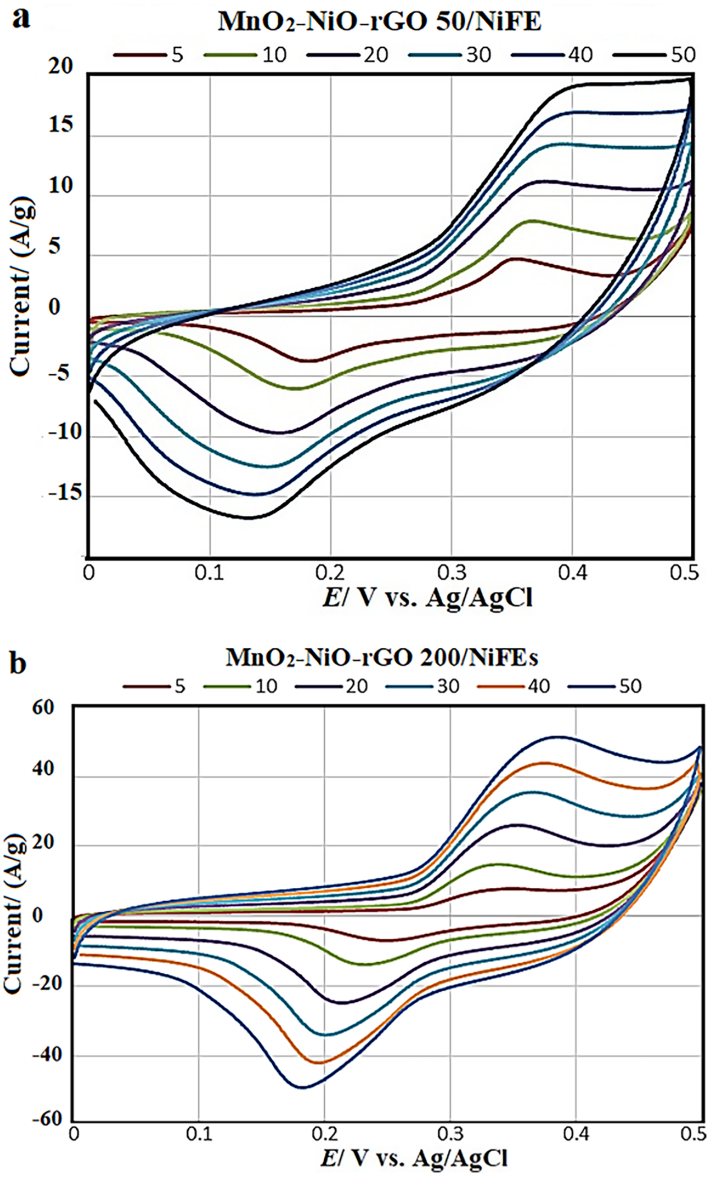


Figure 4: CVs of fabricated electrodes (**a**) MnO_2-NiO–rGO 50/NiFE and (**b**) MnO_2-NiO–rGO 200/NiFEs in 0.1 M KOH solution recorded under various scan rates.

Table 1: Electrochemical capacitance of prepared electrodes.

Electrode	Capacitance F/g
MnO_2-NiO–rGO 50/NiFE	205
MnO_2-NiO–rGO 100/NiFE	235
MnO_2-NiO–rGO 150/NiFE	375
MnO_2-NiO–rGO 200/NiFE	462.5

The electrochemical behavior of the MnO_2-NiO–rGO/NiFE indicates that charge storage results from the combined contribution of electric double-layer capacitance (EDLC) and Faradaic pseudocapacitance. The conductive rGO framework promotes charge accumulation at the electrode/electrolyte interface, contributing to the EDLC component, whereas the distinct redox peaks observed in the CV curves are characteristic of reversible Faradaic reactions involving the nickel- and manganese-based active species in the alkaline electrolyte. These observations suggest that the capacitive performance of the electrode originates from the synergistic interaction of both charge storage mechanisms. A quantitative separation of the EDLC and pseudocapacitive contributions using kinetic analysis methods, such as Dunn's method, was beyond the scope of the present study and will be considered in future investigations [36].

3.2.2 The Charge-Discharge Evaluation

The galvanostat method was used to obtain the specific capacitance of the fabricated electrodes. In this method, a constant current is applied to charge the electrodes until they reach a certain potential. Upon reaching this specified potential (E1), the electrodes are discharged under the same current value until reaching the specified minimum voltage (E2). Then, the plot of potential as a function of time is drawn. An ideal galvanostatic charge/discharge diagram has a symmetrical shape with a constant slope for charge and discharge steps. Real supercapacitors never show linear behavior, and at high currents, the electrical resistance between the electrode components represents a sudden potential drop with the change of current direction. The study of the results of cyclic voltammetry tests showed that MnO_2-NiO–rGO 200/NiFE was better, so this sample was selected as the optimum, and the rest of the tests were performed using it.

MnO_2-NiO–rGO 200/NiFE was tested at currents of 5, 10, 20, and 40 A/g in 2 M KOH solution and their capacities were calculated according to Eq. (3). The results showed that as the current density increases, the capacitance decreases. Also, to investigate the effect of reduced graphene oxide on electrochemical properties and capacitance, a similar electrode without a graphene oxide substrate (MnO_2-NiO 200/NiFE) was fabricated under similar conditions. According to the results (Figs. 5 and 6), the capacitance decreased from 462.5 to 300 F/g (Table 2), which indicates the effect of graphene oxide on the capacitive properties of the supercapacitor. The improvement in the electrochemical performance of the MnO_2-NiO–rGO 200/NiFE can be attributed to the presence of rGO in the composite structure. Due to its good electrical conductivity, rGO provides conductive pathways that facilitate electron transport during the charge-discharge process. In addition, the layered structure of rGO promotes a more uniform distribution of the deposited metal oxides over the nickel foam and increases the contact between the active material and the electrolyte. This structural feature can improve the accessibility of electrochemically active sites and facilitate ion diffusion within the electrode. Furthermore, rGO contributes to charge storage through electric double-layer capacitance, while MnO_2 and NiO mainly provide pseudocapacitive behavior. The combination of these effects is consistent with

the higher specific capacitance obtained for the MnO_2-NiO–rGO 200/NiFE compared with the MnO_2-NiO 200/NiFE prepared under identical experimental conditions.

$$C = \frac{I\Delta t}{m\Delta V} \tag{3}$$

I: Current intensity, ΔV: Potential difference, Δt: Time required for discharge, m: Mass.

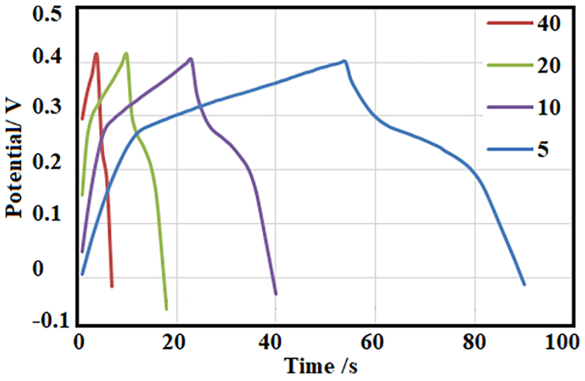


Figure 5: Charge-discharge curve of MnO_2-NiO–rGO 200/NiFE in 2 M KOH solution.

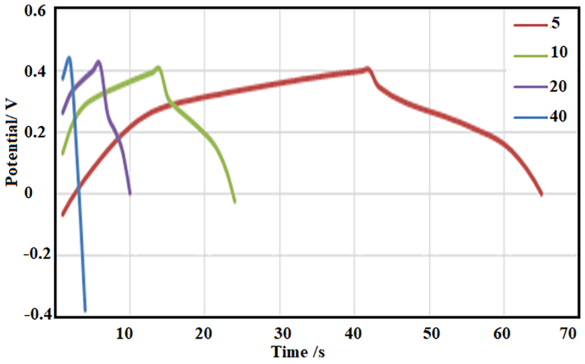


Figure 6: Charge-discharge curve of MnO_2-NiO 200/NiFE in 2 M KOH solution.

Table 2: Electrochemical capacitance of prepared electrodes.

Operating Current Density (A/g)	Specific Capacitance (F/g)	
	MnO_2-NiO-200/NiFE	MnO_2-NiO–rGO 200/NiFE
5	300	462.5
10	275	425
20	250	400
40	200	300

The mass of the deposited active material was determined by weighing the nickel foam substrate before electrodeposition and again after electrodeposition, heat treatment, washing, and complete drying using an

analytical balance. The difference between these two measurements was taken as the active material mass (m) and was used for calculating the specific capacitance according to Eq. (3).

3.2.3 The Stability Evaluation of the MnO_2-NiO–rGO 200/NiFE

One of the most important parameters in evaluating the performance of supercapacitors is cyclic stability, which is evaluated by the galvanostatic method. The stability of MnO_2-NiO–rGO 200/NiFE was investigated by performing galvanostatic charge/discharge tests at a current of 5 A/g. After 1000 consecutive charge and discharge cycles, the capacitance reached 94% of the initial capacity of the electrode, which indicates the good stability of the electrode made of MnO_2-NiO–rGO 200 composite (Fig. 7). Also, sequential cyclic voltammetry of MnO_2-NiO–rGO 200/NiFE was recorded, and the resulting voltammograms indicated the good stability of the electrode even after 1000 cycles.

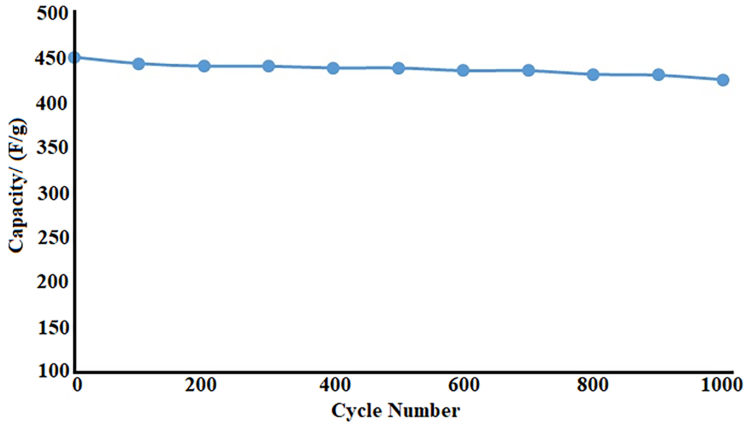


Figure 7: Repeatability and stability of the MnO_2-NiO–rGO 200/NiFE response in 2 M KOH solution.

To provide a more comprehensive evaluation of the fabricated electrode, the electrochemical performance of the MnO_2–NiO–rGO 200/NiFE was compared with recently reported Mn/Ni oxide-based electrodes, as summarized in Table 3. Although the present electrode does not exhibit the highest capacitance among the listed systems, its performance remains competitive with several previously reported electrodes. In addition, the proposed synthesis route is based on a simple electrodeposition procedure followed by a straightforward thermal treatment, which offers advantages in terms of fabrication simplicity and potential cost reduction. The comparison demonstrates that the developed electrode achieves a reasonable balance between electrochemical performance and processing simplicity, highlighting its potential for further optimization in future supercapacitor studies.

Table 3: Performance comparison of MnO_2-NiO–rGO 200/NiFE with reported Mn/Ni oxide-based electrodes for supercapacitors.

Electrode Substrate	Synthesis Method	Electrode Modifier	Electrolyte	Specific Capacitance F/g	Capacitance Performance	Ref.
Ni foam	Chemical	MnO_2	1 M Na_2SO_4	364.1 (at 0.5 A/g)	90.2% (at 3 A/g)	[37]
Graphite sheet	Chemical	MnO_2/NiO	3 M KOH	692 (at 2 A/g)	94.23 (at 2 A/g)	[38]
Graphite plate	Chemical	$Ni(OH)_2$@MnO_2	0.5 M Na_2SO_4	420 (at 1 A/g)	82% (at 10 A/g)	[39]
–	Chemical	Cu@MnO_2	1 M Na_2SO_4	433.15 (at 0.5 A/g)	102.86% (at 20 A/g)	[40]
ITO	Chemical	NiO@rGO	3 M KOH	883 C/g (at 0.5 mV/s)	92.7% (after 35,000 CV cycles)	[41]
Ni foam	Chemical	Fe_3O_4@MnO_2	1 M KOH	715 (at 1 A/g)	85.6 (at 1 A/g)	[42]

(Continued)

Table 3 (continued)

Electrode Substrate	Synthesis Method	Electrode Modifier	Electrolyte	Specific Capacitance F/g	Capacitance Performance	Ref.
FTO	Chemical	MnO_2@NiO@GO	1 M Na_2SO_4	1141 (at 1 A/g)	97.1% (at 2 A/g)	[43]
Graphite electrode	Chemical	MnO_2/NiO (7%)	0.5 M Na_2SO_4	343 (at 1.25 A/g)	83%	[44]
Flexible sponge	Chemical	NiO/MnO_2/CNT	2 M KOH	23 (at 0.1 A/g)	100% (at 1 A/g)	[45]
Ni foam	Chemical	$Ni(OH)_2$/MnO_2	3 M KOH	253.6 (at 2 A/g)	90.5 (at 2 A/g)	[46]
Ni foam	Chemical	MnO_2/$NiCo_2O_4$	6 M KOH	634.4 (at 0.25 A/g)	83.1% (at 1 mA/cm^2)	[47]
Ni foam	Chemical	MnO_2@ Fe-CNF	3 M KOH	924 (at 1 A/g)	75.9% (at 10 A/g)	[48]
Ni foam	Chemical	MnO_2@Co_2NiO_4	3 M KOH	1025 (at 1 A/g)	87% (at 10 A/g)	[49]
FTO	Chemical	Cu_2O@MnO_2 @NiO@SB	1 M Na_2SO_4	1136 (at 1 A/g)	95.24% (at 1 A/g)	[50]
Ni foam	Chemical	Ni-Co-Mn-Ce oxide	3 M KOH	1881.6 (at 4 A/g)	94% (at 15 A/g)	[51]
Ni foam	Chemical	Co_3O_4–$ZnMn_2O_4$/$ZnMnO_3$	6 M KOH	1723.6 C/g (at 1 A/g)	86% (at 10 A/g)	[52]
Cu rod	Electrochem.	MnO_2/GO	1 M Na_2SO_4	829 (at 1 A/g)	81.5% (after 1500 CVs, ν = 50 mV/s)	[29]
Stainless steel plate	Electrochem.	CoO_x/rGO	1 M KOH	608 (at 1 A/g)	–	[30]
Ni foam	Electrochem.	MnO_2-NiO–rGO 200	2 M KOH	462.5 (at 5 A/g)	94% (at 5 A/g)	This Work

GCD: Galvanic charge-discharge
Electrochem: Electrochemical
ITO: Indium Tin Oxide coated glass
FTO: Fluorine-doped Tin Oxide coated glass

3.2.4 EIS Test of the MnO_2-NiO–rGO 200/NiFE

To better and more effectively investigate the electrochemical behavior of supercapacitors, the electrochemical impedance spectroscopy technique was employed. This technique determines the role of various effective parameters, such as the electrical resistance of the electrolyte and electrode materials, charge transfer resistance, in the efficiency of the final supercapacitor. Fig. 8 shows the Nyquist curve of the electrode fabricated at the open circuit potential (−140 mV) in a 2 M KOH solution from a frequency of 0.01 Hz to 100 kHz. The impedance spectrum reveals only a small semicircle in the high-frequency region, indicating that the charge-transfer resistance at the electrode/electrolyte interface is relatively low. This behavior can be attributed to the efficient electrical pathways provided by the MnO_2–NiO–rGO composite together with its good interfacial contact with the nickel foam current collector. As the frequency decreases, the impedance plot approaches a nearly vertical line, which is typical of electrodes with predominantly capacitive characteristics. This response suggests rapid ion transport within the electrode and effective utilization of the electroactive material during the charge–discharge process. Overall, the EIS results demonstrate that the MnO_2–NiO–rGO 200/NiFE electrode possesses favorable charge-transfer kinetics and capacitive behavior, making it a promising electrode material for high-performance supercapacitors.

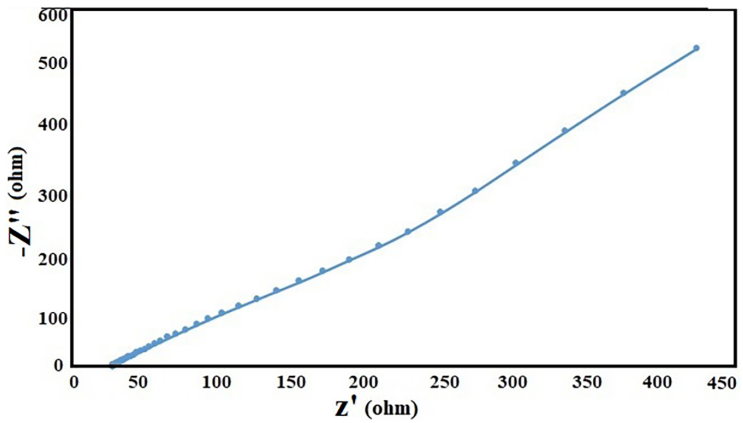


Figure 8: Recorded EIS diagram of MnO_2-NiO–rGO 200/NiFE in 2 M KOH solution.

4 Conclusion

In this project, manganese-nickel double oxide, along with reduced graphene oxide, was successfully deposited on a nickel foam electrode, and after heating, it was converted into MnO_2-NiO–rGO. Using nickel foam as an electrode substrate increased the electrode surface area, porosity, and conductivity of the desired composition. The application of nickel and manganese metal oxide deposition increased the capacitance and Faradaic current of the prepared capacitive system, improved the cyclability, and improved the ion transfer process from the solution to the surface of the final supercapacitor. The cycling test performed in this study provides preliminary information on the electrochemical stability of the MnO_2-NiO–rGO/NiFE. Further studies involving a larger number of charge-discharge cycles, together with structural and morphological characterization after cycling, would provide additional insight into the long-term stability of the electrode and the possible origin of capacitance loss. Also, the use of the one-step electrochemical deposition method has better controllability than other methods and increases the appropriate electrochemical properties. The optimized MnO_2-NiO–rGO/NiF electrode showed a stability of 94% in 1000 voltammetric cycles. In addition, impedance studies revealed the very low charge transfer resistance for the MnO_2-NiO–rGO/NiF electrode, having a capacitance of 462.5 F/g at a current density of 5 A/g.

Acknowledgement: The authors gratefully acknowledge the support of this work by the Shahid Rajaee Teacher Training University, Tehran, Iran.

Funding Statement: This research was funded by Shahid Rajaee Teacher Training University (Grant No: 23905/391033).

Author Contributions: Electrode preparation, formal analysis, investigation, writing—original draft, Hamidreza Mohammad Hoseini; supervision, conceptualization, methodology, visualization, writing—revision and editing, funding acquisition, Masoumeh Ghalkhani; supervision and conceptualization, methodology, editing, Javad Beheshtian; methodology, visualization, editing, Rüstem Keçili. All authors reviewed and approved the final version of the manuscript.

Availability of Data and Materials: The authors confirm that the data supporting the findings of this study are available within the article.

Ethics Approval: Not applicable.

Conflicts of Interest: The authors declare no conflicts of interest.

References

1. Eftekhari A, Shulga YM, Baskakov SA, Gutsev GL. Graphene oxide membranes for electrochemical energy storage and conversion. Int J Hydrogen Energy. 2018;43(4):2307–26. doi:10.1016/j.ijhydene.2017.12.012.
2. Jia H, Cai Y, Lin J, Liang H, Qi J, Cao J, et al. Heterostructural graphene quantum dot/MnO_2 nanosheets toward high-potential window electrodes for high-performance supercapacitors. Adv Sci. 2018;5(5):1700887. doi:10.1002/advs.201700887.
3. Ghalkhani M, Mirzaie RA, Shahmoradi F, Firooz AA. Achievement of an efficient oxygen reduction electrocatalyst based on carbon boosted with MnO_x/$MnCo_2O_4$ with excellent electrocatalytic activity in neutral media. Carbon Lett. 2024;34(1):529–36. doi:10.1007/s42823-023-00599-9.
4. Wu Y, Ghalkhani M, Ashrafzadeh Afshar E, Karimi F, Xia C, Van Le Q, et al. Recent progress in biomass-derived nanoelectrocatalysts for the sustainable energy development. Fuel. 2022;323:124349. doi:10.1016/j.fuel.2022.124349.
5. Karlilar Pata S, Pata UK, Wang Q. Ecological power of energy storage, clean fuel innovation, and energy-related research and development technologies. Renew Energy. 2025;241(6):122377. doi:10.1016/j.renene.2025.122377.
6. Cao J, Emadi A. A new battery/ultracapacitor hybrid energy storage system for electric, hybrid, and plug-in hybrid electric vehicles. IEEE Trans Power Electron. 2012;27(1):122–32. doi:10.1109/TPEL.2011.2151206.
7. Whittingham MS, Savinell RF, Zawodzinski T. Introduction: batteries and fuel cells. Chem Rev. 2004;104(10):4243–4. doi:10.1021/cr020705e.
8. Bollini P, Diwan M, Gautam P, Hartman RL, Hickman DA, Johnson M, et al. Vision 2050: reaction engineering roadmap. ACS Eng Au. 2023;3(6):364–90. doi:10.1021/acsengineeringau.3c00023.
9. Tie SF, Tan CW. A review of energy sources and energy management system in electric vehicles. Renew Sustain Energy Rev. 2013;20(4):82–102. doi:10.1016/j.rser.2012.11.077.
10. Gao Y, Chen S, Han C, Wu G, Wang S, Wang G, et al. An electrochemically rechargeable fuel for continuous operation of electric aircraft and vehicles. Meet Abstr. 2024;MA2024-02(1):179. doi:10.1149/ma2024-021179mtgabs.
11. Munoz-Cupa C, Hu Y, Xu C, Bassi A. An overview of microbial fuel cell usage in wastewater treatment, resource recovery and energy production. Sci Total Environ. 2021;754(40):142429. doi:10.1016/j.scitotenv.2020.142429.
12. Jiao K, Xuan J, Du Q, Bao Z, Xie B, Wang B, et al. Designing the next generation of proton-exchange membrane fuel cells. Nature. 2021;595(7867):361–9. doi:10.1038/s41586-021-03482-7.
13. Kötz R, Carlen M. Principles and applications of electrochemical capacitors. Electrochim Acta. 2000;45(15–16):2483–98. doi:10.1016/S0013-4686(00)00354-6.
14. Yao B, Li M, Zhang J, Zhang L, Song Y, Xiao W, et al. TiN paper for ultrafast-charging supercapacitors. Nano Micro Lett. 2019;12(1):3. doi:10.1007/s40820-019-0340-7.
15. Huang J, Wei J, Xiao Y, Xu Y, Xiao Y, Wang Y, et al. When Al-doped cobalt sulfide nanosheets meet nickel nanotube arrays: a highly efficient and stable cathode for asymmetric supercapacitors. ACS Nano. 2018;12(3):3030–41. doi:10.1021/acsnano.8b00901.
16. He W, Wang C, Li H, Deng X, Xu X, Zhai T. Ultrathin and porous Ni_3S_2/$CoNi_2S_4$ 3D-network structure for superhigh energy density asymmetric supercapacitors. Adv Energy Mater. 2017;7(21):1700983. doi:10.1002/aenm.201700983.
17. Ghalkhani M, Khosrowshahi EM, Sohouli E. Carbon nano-onions: synthesis, characterization, and application. In: Handbook of carbon-based nanomaterials. Amsterdam, The Netherlands: Elsevier; 2021. p. 159–207. doi:10.1016/b978-0-12-821996-6.00006-3.
18. Sohouli E, Adib K, Maddah B, Najafi M. Preparation of a supercapacitor electrode based on carbon nano-onions/manganese dioxide/iron oxide nanocomposite. J Energy Storage. 2022;52(3):104987. doi:10.1016/j.est.2022.104987.
19. Liu L, Zhang X, Liu Y, Gong X. Electrochemical energy storage devices—batteries, supercapacitors, and battery–supercapacitor hybrid devices. ACS Appl Electron Mater. 2025;7(6):2233–70. doi:10.1021/acsaelm.5c00069.
20. Choi C, Robert K, Whang G, Roussel P, Lethien C, Dunn B. Photopatternable hydroxide ion electrolyte for solid-state micro-supercapacitors. Joule. 2021;5(9):2466–78. doi:10.1016/j.joule.2021.07.003.
21. Chen J, Lee PS. Electrochemical supercapacitors: from mechanism understanding to multifunctional applications. Adv Energy Mater. 2021;11(6):2003311. doi:10.1002/aenm.202003311.

22. Zhang J, Chen M. Supercapacitors. In: Chen M, editor. Towards next generation energy storage technologies: from fundamentals to commercial applications. Hoboken, NJ, USA: John Wiley & Sons, Inc.; 2024. p. 331–68. doi:10.1002/9783527845316.ch9.
23. Sun S, Rao D, Zhai T, Liu Q, Huang H, Liu B, et al. Synergistic interface-assisted electrode–electrolyte coupling toward advanced charge storage. Adv Mater. 2020;32(43):2005344. doi:10.1002/adma.202005344.
24. Salanne M, Rotenberg B, Naoi K, Kaneko K, Taberna PL, Grey CP, et al. Efficient storage mechanisms for building better supercapacitors. Nat Energy. 2016;1(6):16070. doi:10.1038/nenergy.2016.70.
25. Kumar N, Kim SB, Lee SY, Park SJ. Recent advanced supercapacitor: a review of storage mechanisms, electrode materials, modification, and perspectives. Nanomater. 2022;12(20):3708. doi:10.3390/nano12203708.
26. Wang H, Casalongue HS, Liang Y, Dai H. $Ni(OH)_2$ nanoplates grown on graphene as advanced electrochemical pseudocapacitor materials. J Am Chem Soc. 2010;132(21):7472–7. doi:10.1021/ja102267j.
27. Xiang C, Li M, Zhi M, Manivannan A, Wu N. A reduced graphene oxide/Co_3O_4 composite for supercapacitor electrode. J Power Sources. 2013;226:65–70. doi:10.1016/j.jpowsour.2012.10.064.
28. Liao Q, Li N, Jin S, Yang G, Wang C. All-solid-state symmetric supercapacitor based on Co_3O_4 nanoparticles on vertically aligned graphene. ACS Nano. 2015;9(5):5310–7. doi:10.1021/acsnano.5b00821.
29. Zhao H, Liu F, Han G, Liu Z, Liu B, Fu D, et al. Co-electrodeposition of MnO_2/graphene oxide coating on carbon paper from phosphate buffer and the capacitive properties. J Solid State Electrochem. 2014;18(2):553–9. doi:10.1007/s10008-013-2291-0.
30. García-Gómez A, Duarte RG, Eugénio S, Silva TM, Carmezim MJ, Montemor MF. Fabrication of electrochemically reduced graphene oxide/cobalt oxide composite for charge storage electrodes. J Electroanal Chem. 2015;755:151–7. doi:10.1016/j.jelechem.2015.07.053.
31. Li Z, Li B, Liao C, Liu Z, Li D, Wang H, et al. One-pot construction of 3-D graphene nanosheets/Ni_3S_2 nanoparticles composite for high-performance supercapacitors. Electrochim Acta. 2017;253(3):344–56. doi:10.1016/j.electacta.2017.09.070.
32. An L, Xu K, Li W, Liu Q, Li B, Zou R, et al. Exceptional pseudocapacitive properties of hierarchical NiO ultrafine nanowires grown on mesoporous NiO nanosheets. J Mater Chem A. 2014;2(32):12799–804. doi:10.1039/c4ta01595a.
33. Xiao H, Qu F, Wu X. Ultrathin NiO nanoflakes electrode materials for supercapacitors. Appl Surf Sci. 2016;360:8–13. doi:10.1016/j.apsusc.2015.10.171.
34. Inamdar AI, Kim Y, Pawar SM, Kim JH, Im H, Kim H. Chemically grown, porous, nickel oxide thin-film for electrochemical supercapacitors. J Power Sources. 2011;196(4):2393–7. doi:10.1016/j.jpowsour.2010.09.052.
35. Chiku M, Toda M, Higuchi E, Inoue H. NiO layers grown on a Ni substrate by galvanostatic anodization as a positive electrode material for aqueous hybrid capacitors. J Power Sources. 2015;286:193–6. doi:10.1016/j.jpowsour.2015.03.095.
36. Augustyn V, Come J, Lowe MA, Kim JW, Taberna PL, Tolbert SH, et al. High-rate electrochemical energy storage through Li^+ intercalation pseudocapacitance. Nat Mater. 2013;12(6):518–22. doi:10.1038/nmat3601.
37. Shen M, Zhu SJ, Liu X, Fu X, Huo WC, Liu XL, et al. Phase and morphology controlled polymorphic MnO_2 nanostructures for electrochemical energy storage. CrystEngComm. 2019;21(35):5322–31. doi:10.1039/c9ce00865a.
38. Meena A, Saleem H, Kumar AS, Shanmugam N, Suganya M. Stoichiometry-balanced MnO_2/NiO nanoscale heterostructures for high-energy and high-power supercapacitors. Inorg Chem Commun. 2026;183(4):115785. doi:10.1016/j.inoche.2025.115785.
39. Tarek YA, Shakil R, Reaz AH, Roy CK, Barai HR, Firoz SH. Wrinkled flower-like rGO intercalated with $Ni(OH)_2$ and MnO_2 as high-performing supercapacitor electrode. ACS Omega. 2022;7(23):20145–54. doi:10.1021/acsomega.2c01986.
40. Jangu S, Kumar S, Deepika KN, Jacob C, Pradhan D. Effect of microwave power and Cu doping on MnO_2 nanostructures and its supercapacitor performance. ACS Appl Electron Mater. 2023;5(6):3078–92. doi:10.1021/acsaelm.3c00152.
41. Rafiq S, Aadil M, Warsi MF, Yousaf S, Alotaibi MT, El-Bahy SM, et al. NiO nanoparticles and their nanohybrid with flat rGO sheets: as an ideal electroactive material for hybrid capacitor applications. Ceram Int. 2022;48(10):14596–605. doi:10.1016/j.ceramint.2022.01.353.

42. Chen Q, Wei W, Tang J, Lin J, Li S, Zhu M. Dopamine-assisted preparation of Fe_3O_4@MnO_2 yolk@shell microspheres for improved pseudocapacitive performance. Electrochim Acta. 2019;317:628–37. doi:10.1016/j.electacta.2019.06.011.
43. Obodo RM, Nsude HE, Eze CU, Okereke BO, Ezugwu SC, Ahmad I, et al. Optimization of MnO_2, NiO and MnO_2@NiO electrodes using graphene oxide for supercapacitor applications. Curr Res Green Sustain Chem. 2022;5(5):100345. doi:10.1016/j.crgsc.2022.100345.
44. Islam MR, Bhuiyan MA, Ahmed MH, Rahaman M. Hydrothermal synthesis of NiO nanoparticles decorated hierarchical MnO_2 nanowire for supercapacitor electrode with improved electrochemical performance. Heliyon. 2024;10(4):e26631. doi:10.1016/j.heliyon.2024.e26631.
45. Peçenek H, Dokan FK, Onses MS, Yılmaz E, Sahmetlioglu E. Highly compressible binder-free sponge supercapacitor electrode based on flower-like NiO/MnO_2/CNT. J Alloys Compd. 2022;913(8):165053. doi:10.1016/j.jallcom.2022.165053.
46. Tian L, Xia K, Wu S, Cai Y, Liu H, Jing X, et al. Rationally design of 2D branched $Ni(OH)_2$/MnO_2 hybrid hierarchical architecture on Ni foam for high performance supercapacitors. Electrochim Acta. 2019;307:310–7. doi:10.1016/j.electacta.2019.03.229.
47. Zhang N, Xu C, Wang H, Zhang J, Liu Y, Fang Y. Assembly of the hierarchical MnO_2@$NiCo_2O_4$ core–shell nanoflower for supercapacitor electrodes. J Mater Sci Mater Electron. 2021;32(2):1787–99. doi:10.1007/s10854-020-04947-7.
48. Tong L, Wu C, Hou J, Yan J, Zhang X, Mu J, et al. Hollow FeOOH nanorods decorated with MnO_2 nanosheets as electrode materials for high-performance asymmetric supercapacitors. J Mater Sci Mater Electron. 2022;33(30):23607–22. doi:10.1007/s10854-022-09120-w.
49. Ren S, Zhang S, Zhang X, Jiang Y, Xu C, Lei Z, et al. Facile growth of Co_2NiO_4 nanowire arrays coating on MnO_2 nanowires for high performance asymmetric supercapacitor applications. J Energy Storage. 2025;128(7):117207. doi:10.1016/j.est.2025.117207.
50. Obodo RM, Nsude HE, Udeh JN, Omugbe E, Ugwuanyi SE, Ezike SC, et al. Enhancement of synergistic effects of Cu_2O@MnO_2@NiO using *Sarcophrynium brachystachys* leaf extract for supercapacitor electrode application. Next Mater. 2024;5(9):100244. doi:10.1016/j.nxmate.2024.100244.
51. Wei C, Cheng C, Shan S, Du W, Wei D, Cheng T, et al. Formation of hybrid NiO-Co_3O_4-MnO_2-CeO_2 hollow spheres as advanced electrode material for high performance supercapacitors. EcoEnergy. 2026;4(1):e70035. doi:10.1002/ece2.70035.
52. Hussain MJ, Ghanem MA, Reddy YVM, Roy N, Mangiri R, Madhavi G. Dandelion-like Co_3O_4/Zn–Mn oxide heterostructures as high-capacity battery-type electrodes for hybrid supercapacitors. Ceram Int. 2026;52(7):8726–39. doi:10.1016/j.ceramint.2026.01.069.